Cell Reports
Physical Science

CellPress
OPEN ACCESS

Article

An engineered coccolith-based hybrid that transforms light into swarming motion

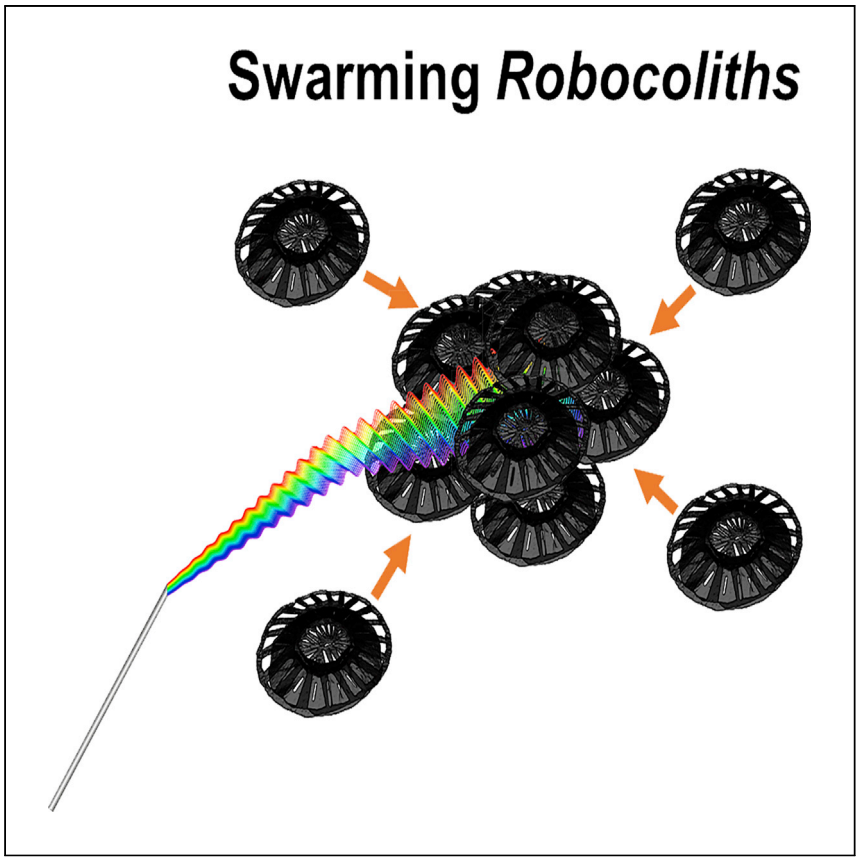

Establishment of controlled nano- and mesoscopic energized entities that gather, in a concerted effort, into motile aggregated patterns is at the forefront of scientific discovery. Lomora et al. report on coccolith-polydopamine hybrids (Robocoliths) that heat and move collectively upon light excitation and accommodate antifouling brushes on their surface.

Mihai Lomora, Aitor Larrañaga, Cesar Rodriguez-Emmenegger, Brian Rodriguez, Ionel Adrian Dinu, Jose-Ramon Sarasua, Abhay Pandit

mihai.lomora@nuigalway.ie (M.L.)
abhay.pandit@nuigalway.ie (A.P.)

HIGHLIGHTS

Coccoliths coated with polydopamine result in design of Robocoliths

Robocoliths control temperature generation and swarming motion under light excitation

The asymmetry of coccoliths is key for generating a net force and directed motion

Robocoliths enable grafting of polymer brushes onto their surface

Lomora et al., Cell Reports Physical Science 2, 100373
March 24, 2021
https://doi.org/10.1016/j.xcrp.2021.100373

Cell Reports
Physical Science

CellPress
OPEN ACCESS

Article

An engineered coccolith-based hybrid that transforms light into swarming motion

Mihai Lomora,[1,2,8,*] Aitor Larrañaga,[1,3] Cesar Rodriguez-Emmenegger,[4] Brian Rodriguez,[5] Ionel Adrian Dinu,[6,7] Jose-Ramon Sarasua,[3] and Abhay Pandit[1,9,10,*]

SUMMARY

Translating energy into swarming motion for miniature entities remains a challenge. This translation requires simultaneously breaking the symmetry of the system to enable locomotion and a coupling effect between the objects that are part of the population to induce the collective motion. Here, we report on Robocoliths, engineered *Emiliania huxleyi (EHUX)* coccolith-based miniature hybrid entities capable of swarming behavior. *EHUX* coccoliths are characterized by an asymmetric morphology that allows breaking symmetry, playing a central role in generating a net force and directed motion. Their activation with the bioinspired material polydopamine not only endows the asymmetric coccoliths with advanced functionalities, such as thermal- and energy-harvesting responsiveness under visible light exposure to display a collective behavior (i.e., swarming), but it also provides a functional surface from which antifouling polymer brushes are grown. In this context, Robocoliths pave the way for the next generation of multifunctional swarming bio-micromachines.

INTRODUCTION

One of the most fundamental questions in science is what defines life.[1] Collective motion is one of the hallmarks of life.[2] This is commonly observed in nature at various dimensional levels as energized entities gather, in a concerted effort, into motile aggregated patterns. These motile aggregated events can be noticed, among many others, as dynamic swarms; e.g., unicellular organisms such as bacteria, locust swarms, or the flocking behavior of birds.[3–5] In contrast to what is accomplished individually, multiple entities enable local interactions between each participant to occur in proximity. If we consider each participant in the collective behavior as a (bio)physical transducer, then the energy will be converted from one type into another. The proxemics will then favor enhanced communication between neighboring individuals via transduction of energy, leading to dynamic and complex synergetic behaviors of the composite powered structure.[6]

Over recent years, fascinating nano- and mesoscopic objects have been designed to collectively move through direct inspiration from nature or by harnessing its existing tools.[7–10] Such robotic swarms were categorized by an online expert panel as among the 10 great unresolved group challenges in the area of robotics.[11] With this in mind, nano- and mesoscopic objects capable of swarming require immediate scientific attention. Although investigation of their underlying mechanism of action is still in its infancy, various systems have been developed that are capable of undergoing controlled and uncontrolled swarming motion by harvesting energy (e.g., light,

[1]CÚRAM, SFI Research Centre for Medical Devices, National University of Ireland Galway, H91 W2TY Galway, Ireland

[2]School of Chemistry, National University of Ireland Galway, University Road, H91 TK33 Galway, Ireland

[3]Department of Mining-Metallurgy Engineering and Materials Science, POLYMAT, Faculty of Engineering Bilbao, University of the Basque Country (UPV/EHU), Plaza Torres Quevedo 1, 48013 Bilbao, Spain

[4]DWI-Leibniz-Institute for Interactive Materials and Institute of Technical and Macromolecular Chemistry, RWTH Aachen University, Forckenbeckstraße 50, 52074 Aachen, Germany

[5]School of Physics and Conway Institute of Biomolecular and Biomedical Research, University College Dublin, Belfield, D04 V1W8 Dublin, Ireland

[6]Department of Functional Polymers, "Petru Poni" Institute of Macromolecular Chemistry, Grigore Ghica Voda Alley 41A, 700487 Iasi, Romania

[7]Department of Chemistry, University of Basel, Mattenstrasse 24a, 4058 Basel, Switzerland

[8]Twitter: @mihailomora

[9]Twitter: @abhay_curam

[10]Lead contact

*Correspondence: mihai.lomora@nuigalway.ie (M.L.), abhay.pandit@nuigalway.ie (A.P.)

https://doi.org/10.1016/j.xcrp.2021.100373

thermal, etc.).[12] Importantly, this energy should be transformed into a net force for the system to move. When the systems of interest are mainly small (meso- to nanoscopic), then their motion, typically at low Reynolds numbers (Re << 1), becomes a very challenging concept.[13] Nevertheless, this demands breaking the symmetry of the system for the locomotion to occur.[14] Furthermore, collective motion requires a coupling effect between the objects that are part of the population.

In this work, the aim is to identify the minimum requirements to design miniature robots (microrobots) with swarming behavior. Therefore, to develop a nano/mesoscopic object capable of swarming behavior, we hypothesize that this object simultaneously fulfills these requirements: (1) it is characterized by broken symmetry with a well-defined morphology, and (2) it is functionalized with a material capable of harvesting energy. If the harvested energy results in a field surrounding the object, and this field can couple with the field of a neighboring object, then the collective behavior will be correlated.

Emiliania huxleyi (*EHUX*) coccolithophore-derived asymmetric coccoliths stand out as candidates for the choice of a nano/mesoscopic object with broken symmetry and well-defined morphology. Besides the thermodynamical stability because of their calcite composition,[15] the critical advantage of *EHUX* coccoliths is their distinctive and sophisticated asymmetric morphology. *EHUX* coccoliths are characterized by several hammer-headed ribs placed to form a proximal and distal disc connected by a central ring. These discs have different sizes but also allow the coccolith to have a curvature, partly resembling a wagon wheel.[16] *EHUX* coccoliths can be isolated from *EHUX* coccolithophores, a unique group of unicellular marine algae that are the primary producers of biogenic calcite in the ocean.[17] Coccolithophores can intracellularly produce intricate three-dimensional mineral structures, such as calcium carbonate scales (i.e., coccoliths), in a process that is driven continuously by a specialized vesicle.[18] After the process is finished, the formed coccoliths are secreted to the cell surface, where they form the exoskeleton (i.e., coccosphere). The broad diversity of coccolith architecture results in further possibilities for specific applications in nanotechnology[19] or biomedicine.[20] Inanimate coccoliths from *EHUX* live coccolithophores, in particular, can be isolated easily in the laboratory with a low culture cost and fast reproductive rate and have a reasonably moderate surface area ($\sim$20 m^2 g^{-1}) exhibiting a mesoporous structure (pore size in the range of 4 nm).[21]

Presumably, if harvesting of energy is done on both sides of the *EHUX* coccolith, then it will allow generation of a net force, which means movement in a directional manner. Coccoliths have immense potential for a multitude of applications, but to enable harvesting of energy, their surface properties must be finely tuned.[22] Inspired by the composition of adhesive proteins in mussels, dopamine self-polymerization into polydopamine is currently the most versatile functionalization strategy for virtually all types of materials.[23] Because of its surface chemistry and wide range of light absorption properties, polydopamine is an ideal choice for aided energy harvesting function on inert substrates.[24–26] In this work, we aim to exploit the benefits of polydopamine coating to provide advanced energy harvesting functionalities to the otherwise inert and inanimate coccoliths. Polydopamine (PDA has already been shown to induce movement of polystyrene beads because of thermal diffusion effects between the object and the surrounding aqueous solution of up to 2°C under near-infrared (NIR) light excitation.[27] However, no collective behavior has been reported. Here, we prove, for the first time, that polydopamine can act as an active component to induce, under visible light (300–600 nm), collective behavior of a

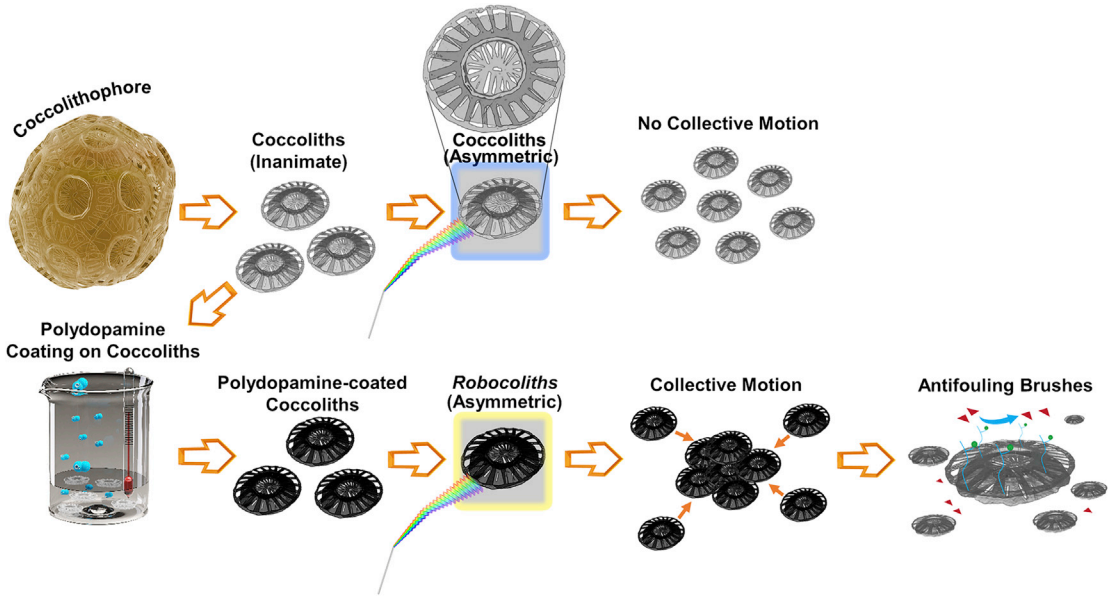

Figure 1. Combination of polydopamine and coccoliths allows design of Robocolith hybrids

EHUX coccolithophores are cultivated for isolation of coccoliths. When coccoliths (asymmetric morphology) are exposed to light, no collective motion is observed. Coccoliths are then mixed gently with dopamine solutions. Thus, polydopamine-coated coccoliths hybrids are obtained as a basis for design of Robocoliths. Light excitation and the asymmetry of Robocoliths generates a thermal flux of heat because of polydopamine's photothermal properties. Coupling of convection from neighboring Robocoliths transforms their movement into an aggregated collective motion. Robocolith functionalization is also proposed to prevent and control nonspecific attachment of biomacromolecules and possible diminution of the aggregation.

structurally complex, natural, and challenging-to-control architecture such as coccoliths. As a result, the organic-inorganic hybrid combination (coccolith-polydopamine) would enable design of Robocoliths.

Dopamine polymerization proceeds in a solution, where it forms small colloidal aggregates that adsorb on the surface of the coccoliths, forming a confluent film. This film is characterized by high roughness, which translates into a high specific surface area and enhanced harvesting of energy. Because of the conjugated nature of the polymer backbone, polydopamine can absorb light over a broad electromagnetic spectrum, including the visible region.

As a result, the surface of coccoliths is endowed with a photothermal effect, locally heating and creating convection induced by the presence of PDA. This local convection is coupled with another nearby local convection, which allows coupling between individual Robocoliths, enabling their collective motion (Figure 1).

Therefore, when the light encounters the anisometric Robocoliths, they heat locally because of the photothermal conversion induced by the presence of PDA on their surface. The intense local heating produces convection that is different on either side of the Robocolith, causing its observed movement. Such convection can couple with the convection of a neighboring Robocolith, resulting in a "swarming" motion. In addition, the surface of Robocoliths is engineered to accommodate antifouling polymer brushes and potentially prevent their aggregation. Although a primary light-activated convective approach is taken as a first step to understand the motion of Robocoliths, a multitude of mechanistic approaches are currently being developed to pave the way for the next generation of multifunctional Robocoliths as swarming bio-micromachines.

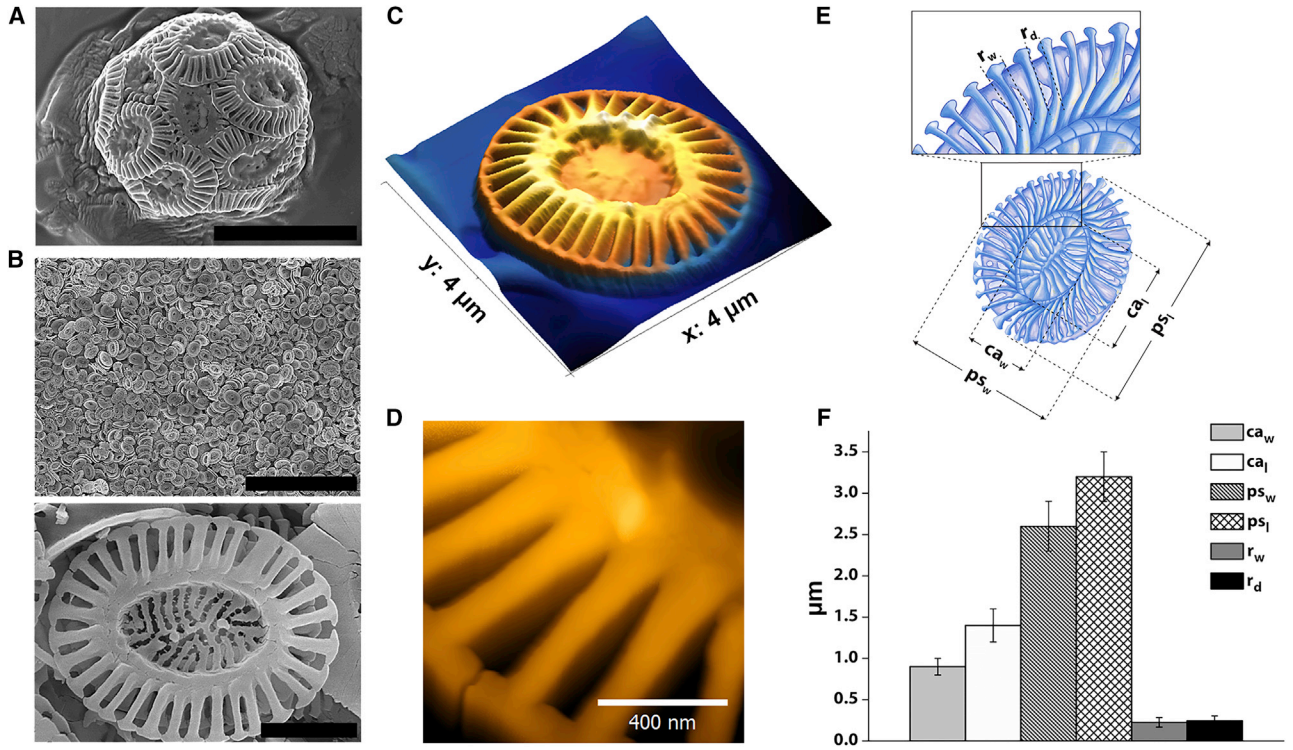

Figure 2. Detailed morphological characterization of coccoliths reveals their fascinating asymmetric architecture

(A) *EHUX* coccolithophores were cultivated successfully and visualized by SEM (scale bar, 4 µm).

(B) Following this, we broke and removed the cellular material from *EHUX* coccolithophores to isolate multiple (top; scale bar, 20 µm) and individual (bottom; scale bar, 1 µm) coccoliths, as visualized by SEM.

(C) AFM image of an individual coccolith. Micrograph size, 4 × 4 µm.

(D) AFM magnification the micrograph of an individual coccolith. Scale bar, 400 nm.

(E) Illustration of a coccolith, depicting its specific morphological parameters.

(F) Typical plotted values of the specific morphological parameters. Data are represented as mean ± SD (n = 55), where n is the number of coccoliths visualized by TEM.

RESULTS AND DISCUSSION

Combination of coccoliths with polydopamine enables design of Robocolith hybrids

To obtain inanimate coccoliths, *EHUX* live coccolithophores were grown in artificial seawater enriched with Guillard's f/10 medium and 10 nM Na_2SeO_3 at an initial density of 50,000 cells mL^{-1}.[28] During exponential growth (10–12 days of culture), *EHUX* microalgae were collected when a density of ~800,000 cells mL^{-1} was reached (Figure S1A). Scanning electron microscopy (SEM) revealed single *EHUX* microalgae during and at the end of the growth phase (Figure S1B; Figure 2A). *EHUX* microalgae were then collected by filtration, and then individual coccoliths were isolated by Triton-NaOCl treatment, followed by several centrifugation/washing steps. Coccoliths were isolated successfully, and their native morphology was preserved during the isolation process (Figure 2B; Figure S1C). Detailed morphological characterization was acquired by atomic force microscopy (AFM) (Figures 2C and 2D). As revealed by transmission electron microscopy (TEM) measurements, each coccolith comprised 32 ± 4 hammer-headed ribs of 230 ± 58 nm width (r_w) that are organized in a ring with a distance (r_d) of 246 ± 56 nm between them. The coccolith central area showed a width (ca_w) and length (ca_l) of 0.90 ± 0.11 µm and 1.42 ± 0.20 µm, respectively, whereas their proximal shield had a width (ps_w) and length (ps_l) of 2.60 ± 0.29 µm and 3.21 ± 0.30 µm, respectively (Figures 2E and 2F).

Coccolith plates are mainly composed of calcium carbonate, as revealed by energy-dispersive X-ray spectroscopy (EDX) coupled with SEM, Fourier transform infrared spectroscopy (FTIR), and X-ray powder diffraction (XRD) (Figure S2). Based on the EDX results, the composition of coccolith plates is very similar to the composition of synthetic calcium carbonate microparticles (Figures S2A and S2B). As observed in the FTIR spectra, the coccoliths are characterized by vibrational bands at 1,394 cm^{-1} (ν_3 asymmetric CO_3 stretch), 870 cm^{-1} (ν_2 asymmetric CO_3 stretch), and 712 cm^{-1} (ν_4 asymmetric CO_3 stretch), whereas the sharp bands at 870 and 712 cm^{-1} are characteristic of calcite. The characteristic FTIR bands are specific to those of synthetic calcium carbonate microparticles,[29] a finding that was confirmed by XRD (Figures S2C and S2D). However, in contrast to the clear calcite coccolith crystal structure, the XRD spectrum of calcium carbonate microparticles mainly revealed vaterite (Figure S2D). Variation in the phase amounts causes the calcium carbonate polymorphs to display unique physicochemical properties, which can also lead to possible thermal instability of the material.[30,31] To investigate this possibility, the coccoliths and the calcium carbonate microparticles were heated to 60°C because this condition was also used to prepare some of the Robocoliths. Interestingly, only the coccolith architecture was preserved upon heating, whereas the calcium carbonate microparticles changed their morphology from round spheres to largely disproportionate patches (Figure S3). Therefore, coccoliths are calcite-based structures with purer crystal composition (better defined/sharper Bragg peaks in XRD) and improved thermal stability compared with synthetic polymorph calcium carbonate microparticles.

The predominant calcium carbonate surface of coccoliths is not readily amenable to covalent functionalization by the usual organic reactions. To circumvent this, we decided to introduce a polydopamine bioinspired functional coating. Polydopamine is a dopamine-derived synthetic eumelanin polymer that contains catechol and amine functionalities in its backbone and has the ability to coat virtually any surface by pure immersion of the substrate in a slightly basic dopamine solution.[23,32,33] Additionally, polydopamine contains quinone ligands, known for their energy-harvesting capabilities.[34] Hence, it can be employed to coat the surface of coccoliths and provide them with energy-harvesting properties while preserving their complex morphology during the functionalization process. However, polymerization of dopamine into polydopamine and substrate coating are time-dependent and -consuming processes that could be reduced considerably by increasing temperature and stirring intensity.[35]

Consequently, we decided to incubate inanimate coccoliths for 1 h at room temperature (RT) in a dopamine hydrochloride solution of 2 mg mL^{-1} in 10 mM Tris buffer (pH 8.5) under mild shaking (2PDAc_RT). The effect of reaction temperature (RT versus 60°C) and dopamine hydrochloride concentration (0.2, 2, 5, and 10 mg mL^{-1}) on polydopamine growth was also investigated by incubating coccoliths in a 10 mM Tris buffer (pH 8.5) solution for 1 h at 60°C. In this respect, we obtained 0.2PDAc, 2PDAc, 5PDAc, and 10PDAc Robocoliths (for more details, see Experimental procedures).

When dopamine is solubilized in 10 mM Tris buffer at basic pH (8.5), it polymerizes over time in films (Figure S4). When coated with polydopamine, Robocoliths were collected by centrifugation, washed thoroughly with distilled water, and characterized by TEM, SEM, X-ray photoelectron spectroscopy (XPS), and EDX (Figure 3; Figure S5). It is noteworthy that application of a polydopamine coating did not affect the nano- or microstructure of the native coccoliths, as shown by electron microscopy

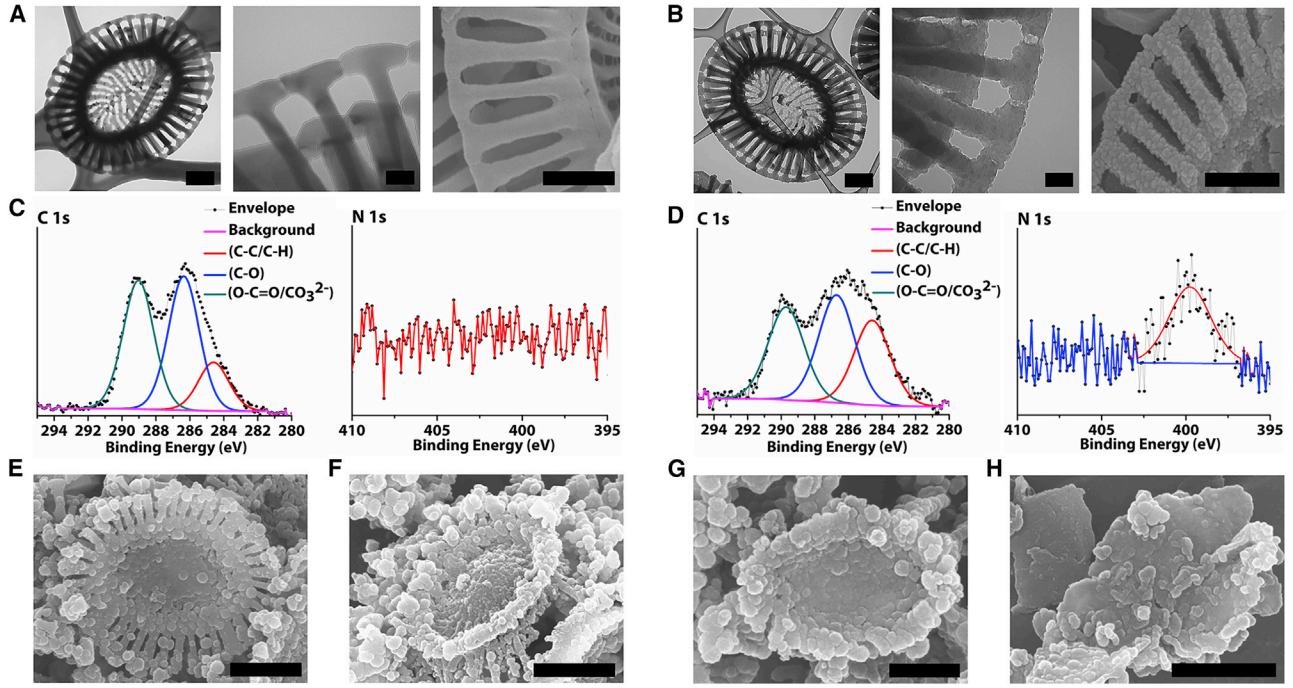

Figure 3. Robocoliths are designed by polydopamine-coccolith hybrid combination

(A) TEM image of pristine coccoliths (left; scale bar, 500 nm) and TEM (center; scale bar, 100 nm) and SEM magnified micrographs of pristine coccoliths (right; scale bar, 500 nm).

(B) TEM images of Robocoliths with 2 mg mL^{-1} dopamine at RT (2PDAc_RT) (left; scale bar, 500 nm; center, scale bar, 100 nm) and magnified SEM micrograph of Robocoliths with 2 mg mL^{-1} dopamine at RT (2PDAc_RT) (right; scale bar, 500 nm).

(C) High-resolution C 1s and N 1s XPS spectra for pristine coccoliths.

(D) High-resolution C 1s and N 1s XPS spectra for 2PDAc_RT Robocoliths.

(E) SEM micrographs of Robocoliths with 0.2 mg mL^{-1} dopamine at 60°C (0.2PDAc). Scale bar, 1 μm.

(F) 2 mg mL^{-1} dopamine at 60°C (2PDAc). Scale bar, 1 μm.

(G) 5 mg mL^{-1} dopamine at 60°C (5PDAc). Scale bar, 500 nm.

(H) 10 mg mL^{-1} dopamine at 60°C (10PDAc). Scale bar, 1 μm.

(Figures 3A and 3B). Only a very thin and homogeneously distributed polymeric coating was observed on the surface of coccoliths for 1 h at RT (Figure 3B). Comparison of the high-resolution C 1s and N 1s orbital spectra of bare and polydopamine-coated coccoliths further proved successful modification of the surface of coccoliths. The C 1s evidenced an increase in contribution at a binding energy of 284.6 eV, stemming from C-C/C-H bonds, whereas a peak centered at 399.8 eV in the N 1s spectra proved the presence of secondary and primary amine groups and imine functionalities, all found in the polydopamine structure (Figures 3C and 3D). EDX analysis of Robocoliths also detected an increase in carbon content up to 29.07 wt % compared with 13.99 wt % for non-coated coccoliths (Figures S2A and S5A).

Furthermore, when coccoliths were prepared at 60°C, almost complete coverage of the surface of coccoliths was obtained with the increase in dopamine concentration (Figures 3E–3H; Figures S5B–S5E). There was also a distinct tendency toward Robocolith aggregation when the dopamine concentration ranged from 2 mg mL^{-1} to 10 mg mL^{-1} when Robocoliths were prepared for 1 h at 60°C (Figures S5F and S5G). Zhou et al.[35] demonstrated previously that a temperature of 60°C does not affect the chemical composition of the final PDA film. Therefore, it appears that the increase in temperature and dopamine concentration indeed leads to an increase in polydopamine deposition and aggregate occurrence without any PDA

chemical perturbance. Moreover, the PDA layer is formed from the surface of coccoliths or by attachment of PDA colloidal aggregates formed in solution.[36] Larger PDA colloidal aggregates contribute to formation of a thicker PDA deposit layer with higher roughness.[37] An increased temperature (i.e., 60°C) will induce the formation of larger colloidal aggregates at a faster rate that will contribute to the PDA layer on the surface of the Robocoliths. The bigger the size of the PDA colloidal aggregates, the higher the probability that one will adhere to another, contributing to the roughness and aggregate occurrence between Robocoliths. Importantly, higher roughness means a higher surface area for Robocoliths to harvest energy.

Robocoliths control temperature generation upon an on and off light excitation mechanism

It is already well known that dopamine polymerization into polydopamine is a process influenced by temperature, catalysts (i.e., oxygen), and pH.[35,38,39] Therefore, it was relevant to identify the role of dissolved oxygen (DO) during dopamine polymerization at RT and 60°C in the absence or presence of coccoliths. When only the buffer (10 mM Tris, pH = 8.5) is heated from RT to 60°C, a decrease in DO is detected from 8.5 $\pm$ 0.03 mg mL^{-1} to 4.3 $\pm$ 0.03 mg mL^{-1} for 10 min (Figure S6A). When the bare coccoliths are dispersed in the buffer, no change in DO content is observed (Figure S6B, purple curve) if the temperature is kept constant at 23°C–24°C (Figure S6B, green curve). Only when dopamine is added to the coccolith dispersion does a noteworthy consumption of DO occurs with its value decreasing from 8.2 $\pm$ 0.01 mg mL^{-1} to 4.2 $\pm$ 0.36 mg mL^{-1} (Figure S6B, orange curve) maintaining a constant temperature for 30 min (Figure S6B, blue curve). Within the same period of 30 min and maintaining the temperature close to 60°C, there is again a barely noticeable variation in DO for bare coccoliths (Figure S6C, purple curve for DO and green curve for temperature), whereas dopamine polymerization induces consumption of DO, with its values dropping from 4.1 $\pm$ 0.14 mg mL^{-1} to 0.6 $\pm$ 0.04 mg mL^{-1} (Figure S6C, orange curve).

The variation in DO concentration during the dopamine polymerization process is more or less similar (i.e., ~4 mg mL^{-1}) at RT and 60°C in the absence or presence of coccoliths. By increasing the temperature of the system, the total initial DO concentration in the system decreases from ~8.2 mg mL^{-1} (RT) to ~4.1 mg mL^{-1} (60°C) (Figure S6B versus S6C). In this case, the decrease in gas solubility can be attributed to the increase in temperature. Thus, at an elevated temperature, there is a decrease in total initial DO concentration in the system. However, the slope of the DO decrease is steeper at 60°C than at RT during the polymerization process. Thus, the rise in temperature leads to an increase in polymerization rate, which translates into higher consumption of oxygen.[40,41]

Robocoliths were then excited at 558 nm (without bright-field [BF] exposure) to investigate the role of temperature using a Pt100 temperature sensor (not displayed), which did not allow use of a BF under the inverted fluorescence microscope (Figure S7). Therefore, dispersions of ~40 mg mL^{-1} 0PDAc, 0.2PDAc, 2PDAc, 5PDAc, and 10PDAc Robocoliths were excited using only the fluorescence filter with excitation at 558 nm over 5 min (Figure S8A). As compared with 0PDAc Robocoliths, which barely displayed any light-induced change in temperature, 0.2PDAc, 2PDAc, 5PDAc, and 10PDAc Robocoliths displayed an increase in temperature. An increase in temperature would normally lead to a decrease in DO into the aqueous environment. All polydopamine-coated Robocoliths displayed a decrease in DO (Figure S8B). Additionally, the DO appears to be correlated with the temperature because an increase in temperature seems to lead to a decrease in DO (Figure S8C).

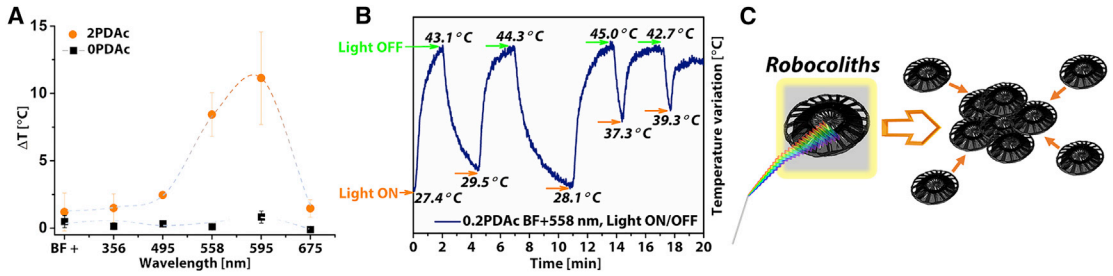

Figure 4. Robocoliths have temperature-generating properties

(A) Change in temperature (ΔT, °C) during light excitation (BF and BF + 356, 495, 558, 595, and 675 nm) of 0PDAc and 2PDAc Robocoliths after 5 min of excitation. Data are represented as mean ± SD (n = 3).

(B) Illustrative variation of 0.2PDAc Robocolith suspension temperature (°C) during manual recordings without light (light off) or during light excitation (light on) under BF + 558 nm for 20 min.

(C) Illustration revealing that the light excitation induces Robocoliths to generate a thermal flux of heat (depicted as a yellow frame) and a force capable of causing motion of the Robocoliths toward a more aggregated, swarm-like scenario (depicted as small orange arrows).

Theoretically, if the DO in the aqueous environment would leave the system, then a decrease in DO content for non-coated Robocoliths could be expected as well. Interestingly, no change in DO was observed for non-coated Robocoliths (0PDAc; Figure S8B). Therefore, the DO consumption upon excitation of Robocoliths, along with the increase in temperature, might be due to the complex chemistry of polydopamine-related oxidative processes.[40,41] The latter will require further research for the mechanistic understanding of these intricate processes upon the excitation of Robocoliths. Because of a possible light on/off switching mechanism, the component units of the complex structure of polydopamine might suffer additional and reversible structural oxidation/re-orientation, allowing consumption of DO. The temperature seems to rise slightly with the increase in initial dopamine concentration used for functionalization of the surface of Robocoliths. Although correlated with the increase in temperature, the decrease in DO is almost the same for the 2PDAc_RT Robocoliths (DO = 7.87 ± 0.38 mg mL^{-1} at 28.49°C ± 0.13°C) as for 2PDAc Robocoliths (DO = 7.97 ± 0.38 mg mL^{-1} at 27.69°C ± 0.29°C) when excited at 558 nm (Figure S8C). Nevertheless, 2PDAc Robocoliths excited at 595 nm displayed a more pronounced decrease in DO, correlating with higher temperature generation (7.71 ± 0.38 mg mL^{-1} at 29.06°C ± 0.78°C), compared with 2PDAc and 2PDAc_RT Robocoliths excited at 558 nm.

Moreover, a thin thermocouple was used (displayed in Figure S7), which allowed use of BF in conjunction with the fluorescence excitation filters (Figure 4A). As a result, 2PDAc Robocoliths showed a gradual increase in temperature with BF + 356, 495, 558 nm; a maximum reached under BF + 595 nm; followed by no variation of temperature at BF + 675 nm. Minimal temperature differences were seen during excitation of bare coccoliths or coccoliths coated with polydopamine under a BF only.

Nevertheless, although a BF slightly influences the outcome of temperature, Robocoliths control temperature via a light switch on/off mechanism. This was illustrated by on/off excitation of ~40 mg mL^{-1} 0.2PDAc Robocoliths under BF + 558 nm for over 15 min (Figure 4B). When the light was on, the temperature increased. When the light was off, the temperature went back to its initial values. The temperature cycle (longer than 13 min) becomes smaller because the fluorescence illumination was turned on and off manually at an earlier time point than with the initial measurements (0–12 min). Thus, the light on-off cycle can also be controlled at temperature levels almost similar to those with a similar irradiation time for up to 1 h (Figure S9). The cycle of controlling the temperature can be repeated several times based on this

light switch on/off mechanism. Therefore, light excitation induces Robocoliths to generate a thermal flux of heat and a force capable of causing motion of the Robocoliths toward a more aggregated, swarm-like scenario (Figure 4C).

Heated Robocoliths display motion upon an on and off light excitation mechanism

Surprisingly, while visualizing polydopamine-coated coccoliths under an inverted fluorescence microscope, we realized that they displayed motion under various excitation wavelengths irrespective of their preparation method (0.2PDAc, 2PDAc, 2PDAc_RT, 5PDAc, and 10PDAc). The wavelengths investigated were 356, 495, 558, 595, and 675 nm, associated with the available fluorescence filters, whereas the BF was used for visualization (see Experimental procedures for details and Figure S7). The velocity of Robocoliths was quantified using a time-resolved particle image velocimetry (PIV) tool in MATLAB. PIV is based on associating directionality vectors using particle movement displayed as colored mapping patterns. By analyzing multiple frames extracted from video recordings, a mean velocity area can be determined.[42] We hypothesized that the motion is a consequence of the PDA photothermal effect on the symmetry-breaking structure of the coccolith. The light-induced movement is also dependent on the asymmetric and intricate architecture of the coccoliths. As an illustration, polydopamine-coated polystyrene spherical beads (bead diameter, 8.5 μm without the coating) were excited with an 808-nm laser to reach an average moving velocity of polydopamine-coated polystyrene beads of approximately 5.5 μm s^{-1} to induce their aggregation for in-solution painting and calligraphy.[27] Unlike single polydopamine-coated polystyrene bead microparticles capable of displaying motion, our Robocoliths display movement under light excitation only in the presence of other Robocoliths.

Formation of PDA aggregates from dopamine is a random process with little to no control over the final morphology (Figure S4). When coccoliths are present, their surface acts as a nucleation interface for PDA aggregates, taking the shape of the coccoliths through polymerization of dopamine on the surface of the coccoliths. Although PDA-coated coccoliths also aggregate to some extent (Figure S5), this phenomenon will have better control over preserving the morphological features of the supporting coccoliths than a random, surface-free, dopamine-to-polydopamine polymerization process. After the Robocoliths are obtained, they are washed repeatedly with distilled water to minimize the presence of unattached PDA aggregates from the surface of coccoliths. Moreover, coccoliths alone do not move under light irradiation, whereas coccoliths coated with PDA do move. This means that the mechanism of motion is not overall heating of the surrounding liquid but an effect associated with PDA itself. As a photothermal material, the function of PDA is to harvest energy to move, so it is expected that PDA aggregates will move as well. To assess the effect of PDA on motion, we compared the speed of 10PDAc Robocoliths with that of 10PDA polydopamine aggregates formed by polymerization of a 10 mg mL^{-1} dopamine solution during 595 nm irradiation while keeping the average concentration of the sample at 40 mg mL^{-1}. Although both samples displayed motion, 57.83 $\pm$ 11.18 μm s^{-1} and 117.92 $\pm$ 30.73 μm s^{-1}, the Robocoliths were twice as fast. This suggests that, although PDA is the source of energy for the motion, the intricate symmetry-breaking morphology of the coccolith also plays a central role in directing the energy for net motion. Conversely, no movement, or hardly any movement, was detected under BF excitation for 10PDA (0.13 $\pm$ 0.02 μm s^{-1}) and 10PDAc (0.16 $\pm$ 0.06 μm s^{-1}) (Figure 5A; Figure S10).

The role of polydopamine in the movement of coccoliths under light excitation was further evidenced by exciting bare coccoliths, compared with Robocoliths, under

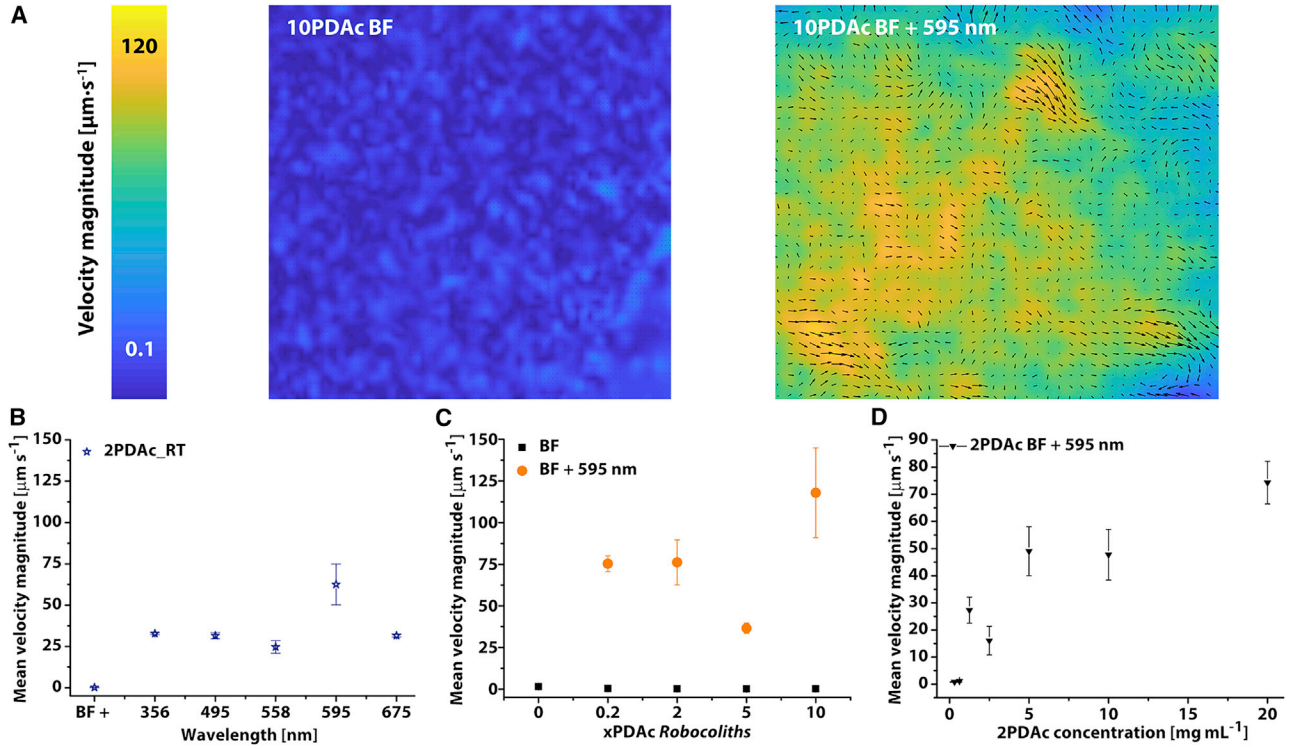

Figure 5. Robocoliths move at impressive speeds

(A) The movement of Robocoliths is associated with vector patterns, and their mean velocities are displayed as color mapping using PIV. As an example, 10PDAc Robocoliths barely move under BF (~0.1 μm s^{-1}, left, 10PDAc BF), whereas under BF and fluorescence excitation (BF + 595 nm), they reach a mean velocity of up to 120 μm s^{-1} (right, 10PDAc BF + 595 nm).

(B) Mean velocity magnitudes of 2PDAc_RT Robocoliths under light excitation with different wavelengths (BF + 356, 495, 558, 595, and 675 nm).

(C) Mean velocity magnitudes of 0PDAc, 0.2PDAc, 2PDAc, 5PDAc, and 10PDAc Robocoliths under BF versus BF + 595 nm.

(D) Mean velocity magnitudes of 2PDAc Robocoliths under BF + 595 nm upon dilution from 20 mg mL^{-1} to 0.3 mg mL^{-1}. Mean velocities were obtained from single videos: X = 3 ± SD, where X = average of 100 images (50 frames) taken at the beginning, middle, and end of each video recording.

various light excitation wavelengths. By exciting ~40 mg mL^{-1} Robocoliths (2PDAc_RT), it was observed that the BF did not influence their movement (0.09 ± 0.01 μm s^{-1}), whereas the velocity varied between 31.55 ± 0.95 and 32.75 ± 0.59 μm s^{-1} when an additional excitation wavelength was added at 356, 495, 558, and 675 nm, reaching a maximum of 62.52 ± 12.33 μm s^{-1} at 595 nm (Figure 5B). Similarly, ~40 mg mL^{-1} 0.2PDAc, 2PDAc, 5PDAc, and 10PDAc Robocoliths also displayed movement upon excitation at 595 nm, with no movement under BF exposure (Figure 5C). At present, more investigation is required to declare a clear correlation between initial dopamine concentration and velocity magnitude. However, in spite of this lack of information, Robocoliths prepared at 60°C generally display higher velocity magnitudes (76.16 ± 13.55 μm s^{-1} for 2PDAc, 595 nm) than Robocoliths prepared at RT (62.52 ± 12.33 μm s^{-1} for 2PDAc_RT, 595 nm) (Figure 5B versus 5C). Presumably, the higher roughness of PDA achievable at a higher temperature may have resulted in a more specific area and a more substantial photothermal effect.

How could temperature affect motion? To assess this, we analyzed the movement of 2PDAc Robocolith samples at 595 nm excitation when the samples were initially at RT or cooled. The first set of samples was placed in a well in the middle of a microplate, whereas for the cooling experiment, the samples were placed in a well in the middle of a microplate and the other wells were filled with ice. Before the

experiment, we allowed the system to equilibrate. No crystallization was observed in the cooled well during the experiment (2PDAc with ice; Figures S11A and S11B). 2PDAc Robocoliths without ice displayed a temperature of 24°C during the experiment. On the other hand, the temperature increased from 0 °C (t = 0 min) up to 15°C (t = 5 min) in the cooled well. Analysis of the mean velocity revealed that Robocoliths that were kept cooled were 40% slower (44.46 $\pm$ 0.5 μm s^{-1}) than the same Robocoliths maintained at RT (76.16 $\pm$ 13.55 μm s^{-1}). The reduction in the velocity may relate to a less efficient photothermal effect at lower temperatures or to a reduction of convection at temperatures lower than RT.

We also analyzed the effect of the numbers of Robocoliths relative to their velocity. For this, we added increasing numbers of Robocoliths to the same volume of water. The velocity was highest for the highest concentration (i.e., ~74 μm s^{-1} at 20 mg mL^{-1}) and decreased with decreasing concentration until 0.3 mg mL^{-1}, beyond which no motion could be observed (~0.8 μm s^{-1}) (Figure 5D). These results highlight a striking finding: the motion of Robocoliths is not only a surface effect but also a cumulative one. We hypothesize that this may be related to the heat transfer mechanism. The higher the number of Robocoliths, the higher the capacity to harvest energy dissipated as heat, which would cause a convective flow amplifying the movement.

Robocoliths transform light into swarming motion

Increasing the number of Robocoliths increases their velocity under irradiation but also aligns the motion in a swarming-like fashion. A higher concentration translates into closer proximity of one Robocolith to another. Because of light-induced photothermal conversion,[43–45] the motion of Robocoliths is enabled, and the likelihood of interaction between adjacent Robocoliths is increased (Video S1). The observation of multiple Robocoliths (0.2PDAc, 2PDAc, 2PDAc_RT, 5PDAc, and 10PDAc) under the BF using the wavelengths investigated therein (356, 495, 558, 595, and 675 nm) reveals their exciting swarming behavior (Figure 6A; Video S2). Negligible movement, if any, was observed for bare, non-coated coccoliths (0PDAc) during their visualization under the BF or the BF and a fluorescence filter. When movement occurred, it was only negligible and was also observed for Robocoliths during their visualization under the BF. Moreover, Robocoliths exhibited motion only when the light was on (in the presence of a fluorescence filter), which stopped immediately when the excitation source (in the absence of a fluorescence filter) was removed (Figure 6B; Video S3). As a result, the polydopamine coating induces swarming of coccoliths. Presumably, the convection flow from one Robocolith may couple with another, and this results in a preferential direction of motion (Figure 6).

Placing and exciting Robocoliths in a microscope well with a glass-bottom dish and a transparent poly(methyl methacrylate) (PMMA) coverslip microplate with a cover lid induces water condensation on the bottom of the dish cover, with evaporation confirming sample heating (Figure S12; Figure 6C; Video S4). No condensation was observed in the absence of excitation (absence of a fluorescence filter). Therefore, the temperature increases in Robocoliths upon light excitation in the presence of a fluorescence filter. The structure-property-function relationship between polydopamine and synthetic eumelanin is markedly similar.[46] Although low, the quantum yield of synthetic eumelanin is strongly dependent on wavelength.[47] Because synthetic eumelanin's optical properties are similar to those of polydopamine, we deduce that polydopamine might only be sensitive to certain wavelengths. The gradient inducing swarming is mainly caused by temperature as an outcome of the light-activated photothermal properties of polydopamine. Therefore, when light

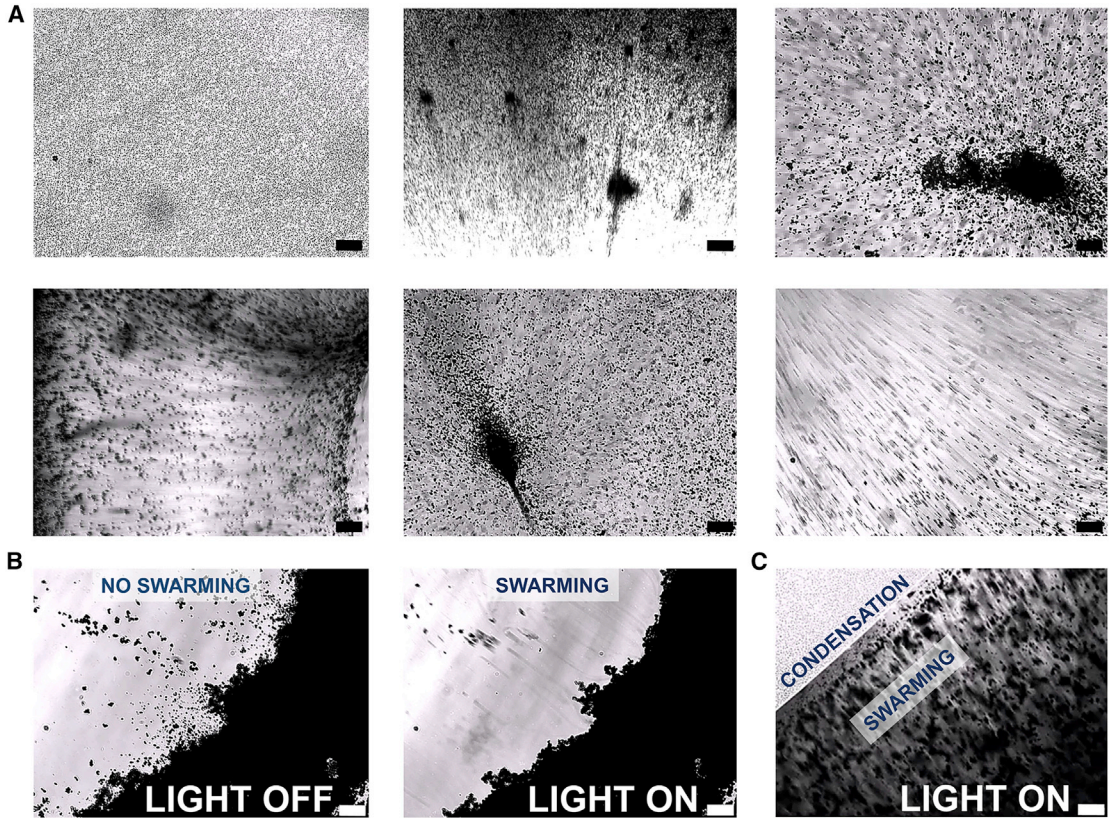

Figure 6. Robocoliths display swarming behavior

(A) Examples of frames extracted from video recordings (Videos S2, S3, and S4) of *EHUX* coccoliths showing no swarming (top row, left) and swarming instances of Robocoliths upon BF and 495 nm excitation: 2PDAc_RT (top row, center), 0.2PDAc (top row, right), 2PDAc (bottom row, left), 5PDAc (bottom row, center), and 10PDAc (bottom row, right). Scale bar, 100 μm.

(B) Robocoliths were visualized under the BF while the light was off (left, light off), and no movement was observed (scale bar, 100 μm). While keeping the BF on and adding a fluorescence filter at 595 nm (right, light on), Robocoliths started to move (scale bar, 100 μm).

(C) Robocoliths were then placed on the glass bottom of a well dish, and the dish was covered with a glass-like polymer coverslip. When the dish containing the Robocoliths was excited at 595 nm (light on), the Robocoliths were not only moving but also inducing condensation on the lower bottom of the dish cover (scale bar, 100 μm).

(BF or any combination of BF + fluorescence filters) shines on bare coccoliths, no temperature increase is observed, and, therefore, no movement is generated (Figure 4A; Video S2). The same situation applies when light (BF only) shines on Robocoliths (PDA-coated coccoliths). However, when light (BF + any combination of fluorescence filters) encounters Robocoliths, then a temperature gradient is formed (Figure 4A), and they swarm (Video S2).

To identify the direction of movement, we analyzed the frames extracted from the videos of swarming Robocoliths at 20, 2.5, and 0.3 mg mL^{-1} (Video S1). Naked-eye observation readily reveals that light-activated Robocoliths tend to move toward the swarm. To confirm this, we analyzed the extracted frames using PIV, in which directionality vectors determined the direction of movement. Under light activation, Robocoliths do indeed move toward the swarm (Figure S13). Mostly static Robocoliths are identified at the lowest concentration (0.3 mg mL^{-1}). Robocoliths at higher concentrations tend to have a higher velocity the farther they are from the swarm (yellow-orange areas). Still, their speed quickly decreases as they bump into each other to form the swarm-like aggregated region (dark blue area).

When polydopamine is applied to the surface of coccoliths, they display swarming during light excitation at neutral pH. Therefore, it was interesting to establish whether the architecture of Robocoliths is preserved under acidic conditions while verifying the swarming effect during light excitation. Robocoliths (2PDAc) were resuspended and kept at RT overnight in the dark in citric acid-Na_2HPO_4 buffer solutions prepared at pH values of 7.3, 5.4, and 3.2 before SEM characterization and movement recordings. As revealed by SEM, the morphology of 2PDAc Robocoliths appeared to be preserved at the specified pH values (Figure S14). Various movement patterns were also observed by resuspending 2PDAc Robocoliths at pH 7.3, 5.4, and 3.2 (Video S5). However, an acidic pH is expected to dissolve the calcium carbonate raw material of Robocoliths.[48] Selective dissolution of coccoliths has already been observed in typical acidification experiments.[49,50] In our case, the buffer solution in which the Robocoliths were incubated is a citric acid-Na_2HPO_4 solution mixture. Although PDA is stable toward citric acid, $CaCO_3$ reacts with this acid, leading to formation of calcium citrate, carbon dioxide, and water.[51,52] Thus, coccoliths will act as a sacrificial template, leaving only a layer of polydopamine in the shape of coccoliths visible by SEM. As a result, an in-depth investigation is required to reveal the influence of pH on the morphology and movement behavior of Robocoliths, and this will be the focus of a follow-up study.

Robocoliths enable grafting of polymer brushes onto their surface

Swarming requires collective movement by coupling fields that generate the force.[53] However, at the microscale, attractive forces between the objects can lead to colloid-like aggregation, ultimately preventing motion. As a possible route to avoid their aggregation and achieve better control over their swarming behavior, we envisage grafting of antifouling and functional polymer brushes onto the surface of coccoliths. Polymer brushes are ultrathin polymer coatings on which polymer chains are tethered from one end to the surface at a very high density. This leads to a stretch conformation that acts as an entropic barrier to protein adsorption.[54] Various brushes have been grafted: gold and even polymeric substrates displaying excellent antifouling properties.[55,56] However, their growth from intricate, inert biological surfaces (i.e., coccoliths) remains very challenging. The lack of functional groups on these types of surfaces often requires drastic activation protocols that transform the surface into a very different material.[57]

Moreover, quite often, the new modification does not yield bonds that are sufficiently strong to account for the high osmotic pressure of the brushes on the surface.[58,59] To overcome this limitation, polydopamine can be employed effectively as an adlayer for immobilization of atom-transfer radical polymerization (ATRP) initiators, as demonstrated by previous experience with poly(ε-caprolactone) (PCL) nanofibrous scaffolds.[60] Polymer brushes based on oligo(ethylene) methacrylates (MeOEGMA) have shown extraordinary abilities for prevention of cell attachment[61,62] and non-specific adsorption of proteins when challenged with real biological fluids.[56] However, MeOEGMA lacks reactive functional groups on its structure, which limits the possibility of further decorating the surface of coccoliths with biomolecules of interest, including antibodies or peptides. Therefore, here we also considered copolymerization of MeOEGMA with small amounts of methacrylic acid (MAA) to provide functional carboxylic groups adequate for enabling subsequent post-polymerization reactions (Figure S15A). From the available approaches used for living copolymerization of MeOEGMA and MAA, including ATRP or reversible addition-fragmentation chain transfer polymerization (RAFT), we selected a "brush-growing" strategy of "grafting from" polymerization reaction via light-induced single-electron transfer living radical polymerization (SET-LRP). This is

because of its widely reported living nature, improved versatility in terms of the broad range of polymerizable monomers using a plethora of solvents, and the fast polymerization kinetics achieved with low catalyst concentrations.[55,63,64] After design of Robocoliths by functionalization of the surface of coccoliths with polydopamine, we covalently immobilized the initiator from which polymer brushes were grown. To decorate the surface of Robocoliths with functional polymer brushes, we first involved the amine moieties provided by the polydopamine layer[41] in the covalent attachment of the radical initiator (2-bromo-2-methylpropionic acid [BMP]) onto the surface of Robocoliths via carbodiimide chemistry. Briefly, the carboxylate groups of 10 μmol of BMP were activated with 12 μmol of N-hydroxysuccinimide (NHS) in the presence of 12 μmol of N-(3-dimethylaminopropyl)-N-ethylcarbodiimide hydrochloride (EDC·HCl) in dimethyl formamide (DMF). After 2 h of mild shaking at RT, 2PDAc_RT Robocoliths (chosen here as an example) were added to the solution mixture along with 4-(dimethylamino)pyridine (DMAP), and the reaction was left overnight at RT. Coccoliths were then collected by centrifugation and washed several times with DMF and distilled water. MeOEGMA and MeOEGMA/MAA (molar ratio of 97.5:2.5) brushes were grown from initiator-coated Robocoliths in a degassed solution of the monomer(s) in DMSO in the presence of $CuBr_2$ and tris [2-(dimethylamino)ethyl]amine (Me_6TREN) and by exposing the reaction system for 1 h to UV light (9-W lamps, λ_{max} = 365 nm) at RT.

Successful conjugation of BMP was evaluated by EDX, where a Br peak appeared after the aforementioned reaction was completed (Figure S15B). According to XPS analysis, the C 1s spectrum of poly(MeOEGMA) brushes grown on coccoliths showed a predominant peak at 286.4 eV stemming from the C-O bonds of ethylene oxide groups in the side chains. In the case of poly(MeOEGMA-co-MAA) brushes, apart from the substantial C-O contribution, an increase of the O-C=O peak was discerned, indicating successful incorporation of MAA into the copolymer structure (Figures S15C and S15D). The surface ζ potential of the coccoliths was also monitored in each reaction step to evaluate formation of brushes (Figure S15E). Bare coccoliths initially showed a negative surface charge value that was kept strongly negative after the polydopamine coating. The negative charge of the coccoliths after polydopamine coating (-24.9 ± 1.0 mV) is associated with the zwitterionic nature of polydopamine, which has an isoelectric point of ~4.[26] Consequently, at pH values above 4, a negative charge is expected because of deprotonation of the phenolic groups. Immobilization of BMP did not result in a significant change of ζ potential, which remained strongly negative at -23.1 ± 0.4 mV. However, after growth of poly(MeOEGMA) polymer brushes, a significant difference in the surface charge of Robocoliths was observed, where the value of the ζ potential was about 0.6 ± 0.1 mV. This almost neutral charge would be beneficial in preventing non-specific electrostatic adhesion of biomolecules. Although the neutral brushes lack ionic stabilization, they provide steric stabilization for the Robocoliths. Finally, Robocoliths functionalized with poly(MeOEGMA-co-MAA) brushes displayed a slightly negative charge (-2.8 ± 0.3 mV), which agrees well with the presence of carboxylate groups. Thermogravimetric analysis (TGA) also confirmed successful polymerization of poly(MeOEGMA) and poly(MeOEGMA-co-MAA) brushes onto the surface of Robocoliths (Figure S15F). In the studied temperature range, bare coccoliths and 2PDAc_RT Robocoliths did not suffer significant weight loss (<3%). In contrast, 25% and 16% weight loss was seen for the Robocoliths functionalized with poly(MeOEGMA) and poly(MeOEGMA-co-MAA), respectively. Considering the surface area of coccoliths reported in the literature (i.e., 20 $m^2 g^{-1}$),[21] this represents a surface density of ~1,666 ng cm^{-2} and ~952 ng cm^{-2} for poly(MeOEGMA) and poly(MeOEGMA-co-MAA) brushes, respectively.

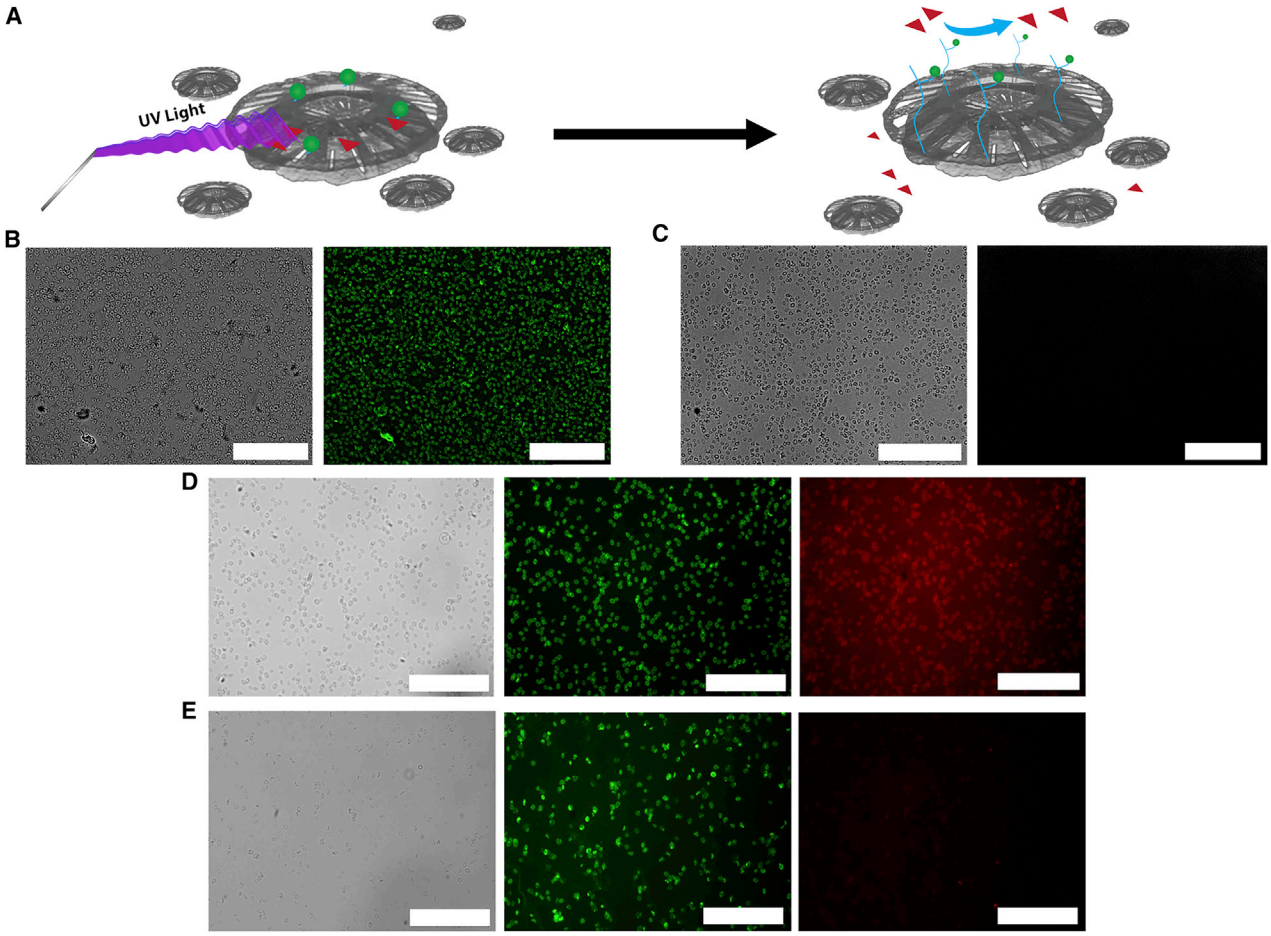

Figure 7. The Robocolith surface allows growth of antifouling brushes

(A) Schematic representation of the interaction between antifouling Robocoliths with fluorescently labeled proteins.

(B) BF and the corresponding fluorescence micrographs of 2PDAc_RT Robocoliths incubated with FITC-BSA. Scale bars, 50 μm.

(C) BF and the corresponding fluorescence micrographs of poly(MeOEGMA) brush-modified 2PDAc_RT Robocoliths incubated with FITC-BSA. Scale bars, 50 μm.

(D) BF and fluorescent micrographs of 2PDAc_RT Robocoliths incubated with FITC-BSA and TRITC-BSA. Scale bars, 50 μm.

(E) BF and fluorescence micrographs of poly(MeOEGMA-co-MAA) brush-modified 2PDAc_RT Robocoliths incubated with FITC-BSA and TRITC-BSA. Scale bars, 50 μm.

We further assessed the adsorption of proteins on 2PDAc_RT Robocoliths (control) and polymer brush-coated 2PDAc_RT Robocoliths (Figure 7). Both systems were incubated in fluorescein isothiocyanate-labeled albumin solution (FITC-BSA) (1 mg mL^{-1}) for 1 h under mild shaking. The albumin model protein was adsorbed onto the surface of Robocoliths, as demonstrated by fluorescence microscopy (Figure 7B). In contrast, no FITC-BSA was detected on poly(MeOEGMA) brush-modified Robocoliths, indicating prevention of non-specific adsorption of proteins (Figure 7C).

To provide functionalities for the structure of polymer brushes, a small amount (2.5 mol %) of MAA was incorporated. Poly(MeOEGMA-co-MAA) brushes were also able to reduce adsorption of FITC-BSA in comparison with Robocoliths (~60% reduction in fluorescent intensity), but the reduction in fluorescence intensity was not as efficient as in the case of poly(MeOEGMA) brushes. This could be ascribed to the interactions (e.g., electrostatic or hydrogen bonding) between the free carboxylic acids from the polymer brush and the functional groups of the

protein. However, after activating the carboxylic groups of poly(MeOEGMA-co-MAA) brushes via carbodiimide chemistry, further conjugation reactions with the biomolecule of interest (i.e., FITC-BSA) were allowed, as demonstrated by the increase in fluorescence intensity (Figure S16).

To prove specific conjugation of the biomolecule of interest in Robocoliths functionalized with poly(MeOEGMA-co-MAA) brushes, Robocoliths were first incubated with FITC-BSA, followed by incubation with tetramethylrhodamine isothiocyanate-labeled bovine serum albumin (TRITC-BSA). Both fluorescently labeled BSAs were absorbed on the surface of Robocoliths. Therefore, use of polydopamine as a surface layer may be a severe drawback when highly specific interaction with biomolecules of interests is desired (Figure 7D).

Accordingly, Robocoliths functionalized with activated poly(MeOEGMA-*co*-MAA) brushes were first incubated with FITC-BSA when the protein was covalently coupled onto the surface, followed by incubation with TRITC-BSA. Robocoliths functionalized with activated poly(MeOEGMA-co-MAA) brushes showed no further adsorption of TRITC-BSA. Therefore, coccoliths decorated with poly(MeOEGMA-co-MAA) brushes preserve their antifouling nature and facilitate specific conjugation of the biomolecule of interest (Figure 7E). Robocoliths functionalized with poly(MeOEGMA) did not allow protein fouling. Moreover, poly(MeOEGMA) lacks functionalities that will enable further conjugation reactions. By introducing MAA, part of the antifouling ability of the poly(MeOEGMA) Robocoliths is impaired slightly. However, poly(MeOEGMA-co-MAA) Robocoliths display carboxylic groups, which, after being activated via carbodiimide chemistry, can enable further conjugation and specific reactions with the biomolecules of interest. Therefore, the antifouling properties of functionalized Robocoliths could then be checked in respect to other bio(macro)molecules. This model is tunable because it can be developed toward target proteins of interest while avoiding attachment of other proteins.

Overall, coccoliths from *EHUX* were cultured easily in the laboratory, with fast growth rates and reproducible nanostructured asymmetric morphologies with potential for nanotechnology applications.[20,65] Coccoliths are microscopic asymmetrical objects, enabling motion at low Reynolds numbers[66] while ensuring breaking of the symmetry for improved swarming ability. It is essential to note that coccoliths were described recently as micro-photo-regulators in the presence of an electromagnetic wave, such as light,[67] making the coccolith an exciting choice for designing Robocoliths. Moreover, polydopamine has been shown to induce a controlled light-responsive swarming behavior in coccoliths. This enabled design of a novel Robocolith with intricate architectural stability, temperature-generating properties, and motion with velocities of up to 120 $\mu m\ s^{-1}$.

Previous studies have revealed that an increased reaction temperature (i.e., 60°C) leads to a surface-deposited polydopamine layer with higher roughness in a shorter period of time (<8 h) than those prepared at RT for 24 h.[35] This suggests that Robocoliths prepared using the same concentration of dopamine will have higher surface roughness when prepared at 60°C (2PDAc) than those prepared at RT (2PDAc_RT). Moreover, the increase in dopamine concentration at a constant temperature leads to polydopamine films with increased thickness, roughness, and absorbance.[68] This also suggests that, by increasing the initial concentration of dopamine, our Robocoliths prepared at 60°C resulted in PDA layers of an assumed increased roughness; 0.2 PDAc Robocoliths had the lowest PDA roughness, and 10 PDAc Robocoliths had the highest PDA roughness. Increased PDA thickness on the surface of

Robocoliths also leads to a higher surface area and increased ability to harvest light. Thus, the preparation conditions change the Robocoliths' ability to harvest energy, which, in turn, is reflected by their velocity under light excitation (BF + 595 nm); 2PDAc_RT Robocoliths move slower (62.52 $\pm$ 12.33 μm s^{-1}) than 2PDAc Robocoliths (76.16 $\pm$ 13.55 μm s^{-1}) and slower than 10PDAc Robocoliths (117.92 $\pm$ 30.73 μm s^{-1}). However, use of a higher temperature of reaction and higher initial concentration of dopamine also results in a higher amount of PDA colloidal aggregates, which is difficult to control and might have a direct effect on the uniformity of the distributed PDA on the surface of Robocoliths and, thus, on our observations.

Asymmetric particles with differently responsive sides to environmental stimuli (e.g., Janus particles covering different metals on the two sides) can generate net propulsion forces to generate movement.[69] We also acknowledge that, in light-driven motion, the particles can be spherical, and light shading can also make a spherical particle into a Janus particle.[70] Nevertheless, published reports have demonstrated that an asymmetric shape plays an important part in breaking the symmetry and generating propulsion forces.[71–73] It has been reported that, at high concentrations of light-activated, polydopamine-coated, spherical polystyrene beads, competition between forces generated by thermal buoyancy influenced their movement.[27] In contrast, the coccoliths' asymmetric morphology should allow asymmetric distribution of thermal gradients, enhancing this phenomenon. Unlike single polydopamine-coated polystyrene beads microparticles capable of displaying motion,[27] our Robocoliths enable movement under light excitation only in the presence of other Robocoliths. Moreover, compared with polydopamine-coated polystyrene bead microparticles,[27] the asymmetric coccolith has an architecture that is far more challenging to control. The coccolith's high surface area also allows more PDA to be attached to its surface. Therefore, a higher energy-harvesting capability, coupled with a higher probability of the occurrence of PDA-specific reversible hydrogen bonding/π-π interaction, enables the observed swarming-like effect.

More studies of the role of excitation, coccolith properties, the polydopamine layer and its polymerization parameters (i.e., oxygen, pH, and temperature), and the role of antifouling brush accommodation capacity with respect to swarming ability should be considered. With this, a better understanding of the swarming mechanism of Robocoliths under light excitation will be obtained.

EXPERIMENTAL PROCEDURES

Resource availability

Lead contact

All data required to evaluate the conclusions in the paper are present in the Supplemental experimental procedures. Further information and requests for resources and reagents should be directed to and will be fulfilled by the lead contact, Abhay Pandit (abhay.pandit@nuigalway.ie).

Materials availability

This study did not generate new unique materials.

Data and code availability

This study did not generate/analyze datasets/code.

SUPPLEMENTAL INFORMATION

Supplemental information can be found online at https://doi.org/10.1016/j.xcrp.2021.100373.

ACKNOWLEDGMENTS

The authors thank SGIker of UPV/EHU, the European Regional Development Fund (ERDF), and the European Social Fund (ESF) for technical and human support. M.L. thanks Dr. Gerard O'Connor (NUI Galway, Ireland) for beneficial scientific discussions related to this work. A.L. and M.L. thank Gillian Murphy (NUI Galway) for maintenance/extraction of coccoliths. M.L. is grateful for the help and input of his student, David Shumate (Georgia Tech, Atlanta, GA, USA). M.L. is also very thankful for support received from PreSens Precision Sensing GmbH (Regensburg, Germany) regarding proper handling and use of the oxygen and temperature probes and data analysis. M.L. would particularly like to thank Pierce Lalor, Dr. Emma McDermott, and Dr. Eadaoin Timmins (NUI Galway) for invaluable support with electron microscopy. Additionally, the authors acknowledge the aforementioned for access to facilities and the scientific and technical assistance kindly offered by the experts of the Centre for Microscopy & Imaging at the National University of Ireland Galway (www.imaging.nuigalway.ie). We also acknowledge Drawinginc (https://drawinginc.ie/) and Maciej Doczyk for support with preparation of the schematics. Anthony Sloan is recognized for help with language edits. Finally, we acknowledge the editorial assistance of Dr. Raghvendra Bohara. This publication has emanated from research supported in part by a grant from Science Foundation Ireland (SFI) and the European Regional Development Fund (ERDF) under grant 13/RC/2073_P2. A.L. and J.R.S. are thankful for funding from the Basque Government, Department of Education (IT-927-16). A.L. acknowledges the Basque Government for a postdoctoral grant (POS_2014_1_26). Support from the Spanish Ministry of Industry and Competitiveness for project MAT 2013-45559-P is also acknowledged. A.P., C.R.-E., and J.R.S. would like to acknowledge funding from the European Cooperation in Science and Technology (COST) Action iPROMEDAI project (TD1305). M.L. gratefully acknowledges his Early Postdoctoral Mobility Fellowship from the Swiss National Science Foundation (P2BSP3_174974).

AUTHOR CONTRIBUTIONS

Conceptualization, M.L., A.L., C.R.-E., I.A.D., and A.P.; methodology, validation, formal analysis, investigation, and writing – original draft, M.L. and A.L.; resources, M.L., B.R., and A.P.; writing – review & editing, M.L., A.L., C.R.-E., B.R., I.A.D., J.-R.S., and A.P.; visualization, M.L.; supervision, M.L. and A.P.; project administration and funding acquisition, M.L. and A.P.

DECLARATION OF INTERESTS

The authors declare no competing interests.

Received: August 7, 2020
Revised: January 18, 2021
Accepted: February 19, 2021
Published: March 16, 2021

REFERENCES

1. Allen, R.E., and Lidström, S. (2017). Life, the Universe, and everything - 42 fundamental questions. Phys. Scr. *92*, 1–41.
2. Vicsek, T., and Zafeiris, A. (2012). Collective motion. Phys. Rep. *517*, 71–140.
3. Darnton, N.C., Turner, L., Rojevsky, S., and Berg, H.C. (2010). Dynamics of bacterial swarming. Biophys. J. *98*, 2082–2090.
4. Topaz, C.M., D'Orsogna, M.R., Edelstein-Keshet, L., and Bernoff, A.J. (2012). Locust dynamics: behavioral phase change and swarming. PLoS Comput. Biol. *8*, e1002642.
5. Corcoran, A.J., and Hedrick, T.L. (2019). Compound-V formations in shorebird flocks. eLife *8*, 1–18.
6. Herpich, T., Thingna, J., and Esposito, M. (2018). Collective power: Minimal model for thermodynamics of nonequilibrium phase transitions. Phys. Rev. X *8*, 1–20.
7. Abendroth, J.M., Bushuyev, O.S., Weiss, P.S., and Barrett, C.J. (2015). Controlling motion at the nanoscale: Rise of the molecular machines. ACS Nano *9*, 7746–7768.
8. Wang, W., Duan, W., Ahmed, S., Mallouk, T.E., and Sen, A. (2013). Small power: Autonomous nano- and micromotors

propelled by self-generated gradients. Nano Today *8*, 531–554.

9. Zhang, J., Guo, J., Mou, F., and Guan, J. (2018). Light-controlled swarming and assembly of colloidal particles. Micromachines (Basel) *9*, 1–18.

10. Di Leonardo, R. (2016). Active colloids: Controlled collective motions. Nat. Mater. *15*, 1057–1058.

11. Yang, G.-Z., Bellingham, J., Dupont, P.E., Fischer, P., Floridi, L., Full, R., Jacobstein, N., Kumar, V., McNutt, M., Merrifield, R., et al. (2018). The grand challenges of *Science Robotics*. Sci. Robot. *3*, 1–14.

12. Wang, W., Duan, W., Ahmed, S., Sen, A., and Mallouk, T.E. (2015). From one to many: dynamic assembly and collective behavior of self-propelled colloidal motors. Acc. Chem. Res. *48*, 1938–1946.

13. Nelson, P.C. (2003). Life in the slow lane: The low Reynolds-number world. In Biological Physics: Energy, Information, Life (W.H. Freeman), pp. 158–194.

14. Brooks, A.M., Sabrina, S., and Bishop, K.J.M. (2018). Shape-directed dynamics of active colloids powered by induced-charge electrophoresis. Proc. Natl. Acad. Sci. USA *115*, E1090–E1099.

15. Karunadasa, K.S.P., Manoratne, C.H., Pitawala, H.M.T.G.A., and Rajapakse, R.M.G. (2019). Thermal decomposition of calcium carbonate (calcite polymorph) as examined by in-situ high-temperature X-ray powder diffraction. J. Phys. Chem. Solids *134*, 21–28.

16. Zhai, P.-W., Hu, Y., Trepte, C.R., Winker, D.M., Josset, D.B., Lucker, P.L., and Kattawar, G.W. (2013). Inherent optical properties of the coccolithophore: Emiliania huxleyi. Opt. Express *21*, 17625–17638.

17. Bolton, C.T., Hernández-Sánchez, M.T., Fuertes, M.-Á., González-Lemos, S., Abrevaya, L., Mendez-Vicente, A., Flores, J.-A., Probert, I., Giosan, L., Johnson, J., and Stoll, H.M. (2016). Decrease in coccolithophore calcification and CO_2 since the middle Miocene. Nat. Commun. *7*, 10284.

18. Meldrum, F.C., and Cölfen, H. (2008). Controlling mineral morphologies and structures in biological and synthetic systems. Chem. Rev. *108*, 4332–4432.

19. Skeffington, A.W., and Scheffel, A. (2018). Exploiting algal mineralization for nanotechnology: bringing coccoliths to the fore. Curr. Opin. Biotechnol. *49*, 57–63.

20. Lomora, M., Shumate, D., Rahman, A.A., and Pandit, A. (2019). Therapeutic applications of phytoplankton, with an emphasis on diatoms and coccolithophores. Adv. Ther. (Weinh.) *2*, 1–24.

21. Jakob, I., Chairopoulou, M.A., Vučak, M., Posten, C., and Teipel, U. (2017). Biogenic calcite particles from microalgae-Coccoliths as a potential raw material. Eng. Life Sci. *17*, 605–612.

22. Kim, S.H., Nam, O., Jin, E., and Gu, M.B. (2019). A new coccolith modified electrode-based biosensor using a cognate pair of aptamers with sandwich-type binding. Biosens. Bioelectron. *123*, 160–166.

23. Lee, H., Dellatore, S.M., Miller, W.M., and Messersmith, P.B. (2007). Mussel-inspired surface chemistry for multifunctional coatings. Science *318*, 426–430.

24. Ryu, J.H., Messersmith, P.B., and Lee, H. (2018). Polydopamine surface chemistry: A decade of discovery. ACS Appl. Mater. Interfaces *10*, 7523–7540.

25. Schanze, K.S., Lee, H., and Messersmith, P.B. (2018). Ten years of polydopamine: Current status and future directions. ACS Appl. Mater. Interfaces *10*, 7521–7522.

26. Liu, Y., Ai, K., and Lu, L. (2014). Polydopamine and its derivative materials: synthesis and promising applications in energy, environmental, and biomedical fields. Chem. Rev. *114*, 5057–5115.

27. Sun, Y., Liu, Y., Zhang, D., Zhang, H., Jiang, J., Duan, R., Xiao, J., Xing, J., Zhang, D., and Dong, B. (2019). Calligraphy/painting based on a bioinspired light-driven micromotor with concentration-dependent motion direction reversal and dynamic swarming behavior. ACS Appl. Mater. Interfaces *11*, 40533–40542.

28. Paasche, E., Brubak, S., Skattebøl, S., Young, J.R., and Green, J.C. (1996). Growth and calcification in the coccolithophorid Emiliania huxleyi (Haptophyceae) at low salinities. Phycologia *35*, 394–403.

29. Larrañaga, A., Isa, I.L.M., Patil, V., Thamboo, S., Lomora, M., Fernández-Yague, M.A., Sarasua, J.-R., Palivan, C.G., and Pandit, A. (2018). Antioxidant functionalized polymer capsules to prevent oxidative stress. Acta Biomater. *67*, 21–31.

30. Kontoyannis, C.G., and Vagenas, N.V. (2000). Calcium carbonate phase analysis using XRD and FT-Raman spectroscopy. Analyst (Lond.) *125*, 251–255.

31. Ogino, T., Suzuki, T., and Sawada, K. (1987). The formation and transformation mechanism of calcium carbonate in water. Geochim. Cosmochim. Acta *51*, 2757–2767.

32. Fernandez-Yague, M.A., Larrañaga, A., Gladkovskaya, O., Stanley, A., Tadayyon, G., Guo, Y., Sarasua, J.-R., Tofail, S.A.M., Zeugolis, D.I., Pandit, A., and Biggs, M.J. (2015). Effects of polydopamine functionalization on boron nitride nanotube dispersion and cytocompatibility. Bioconjug. Chem. *26*, 2025–2037.

33. Larrañaga, A., Ramos, D., Amestoy, H., Zuza, E., and Sarasua, J.-R. (2015). Coating of bioactive glass particles with mussel-inspired polydopamine as a strategy to improve the thermal stability of poly(l -lactide)/bioactive glass composites. RSC Advances *5*, 65618–65626.

34. Son, E.J., Kim, J.H., Kim, K., and Park, C.B. (2016). Quinone and its derivatives for energy harvesting and storage materials. J. Mater. Chem. A Mater. Energy Sustain. *4*, 11179–11202.

35. Zhou, P., Deng, Y., Lyu, B., Zhang, R., Zhang, H., Ma, H., Lyu, Y., and Wei, S. (2014). Rapidly-deposited polydopamine coating via high temperature and vigorous stirring: formation, characterization and biofunctional evaluation. PLoS ONE *9*, e113087.

36. Pop-Georgievski, O., Verreault, D., Diesner, M.-O., Proks, V., Heissler, S., Rypáček, F., and Koelsch, P. (2012). Nonfouling poly(ethylene oxide) layers end-tethered to polydopamine. Langmuir *28*, 14273–14283.

37. Pop-Georgievski, O., Popelka, Š., Houska, M., Chvostová, D., Proks, V., and Rypáček, F. (2011). Poly(ethylene oxide) layers grafted to dopamine-melanin anchoring layer: stability and resistance to protein adsorption. Biomacromolecules *12*, 3232–3242.

38. Salomäki, M., Marttila, L., Kivelä, H., Ouvinen, T., and Lukkari, J. (2018). Effects of pH and oxidants on the first steps of polydopamine formation: A thermodynamic approach. J. Phys. Chem. B *122*, 6314–6327.

39. Bernsmann, F., Ball, V., Addiego, F., Ponche, A., Michel, M., Gracio, J.J.A., Toniazzo, V., and Ruch, D. (2011). Dopamine-melanin film deposition depends on the used oxidant and buffer solution. Langmuir *27*, 2819–2825.

40. Du, X., Li, L., Li, J., Yang, C., Frenkel, N., Welle, A., Heissler, S., Nefedov, A., Grunze, M., and Levkin, P.A. (2014). UV-triggered dopamine polymerization: control of polymerization, surface coating, and photopatterning. Adv. Mater. *26*, 8029–8033.

41. Liebscher, J. (2019). Chemistry of Polydopamine - Scope, Variation, and Limitation. Eur. J. Org. Chem. *2019*, 4976–4994.

42. Thielicke, W., and Stamhuis, E. (2014). PIVlab – Towards user-friendly, affordable and accurate digital particle image velocimetry in MATLAB. J. Open Res. Softw. *2*, e30.

43. Meng, F., Hao, W., Yu, S., Feng, R., Liu, Y., Yu, F., Tao, P., Shang, W., Wu, J., Song, C., and Deng, T. (2017). Vapor-enabled propulsion for plasmonic photothermal motor at the liquid/air Interface. J. Am. Chem. Soc. *139*, 12362–12365.

44. Yang, R.-L., Zhu, Y.-J., Chen, F.-F., Qin, D.-D., and Xiong, Z.-C. (2019). Superhydrophobic photothermal paper based on ultralong hydroxyapatite nanowires for controllable light-driven self-propelled motion. ACS Sustain. Chem. Eng. *7*, 13226–13235.

45. Zhang, L., Zhang, H., Liu, M., and Dong, B. (2016). Reprogrammable logic gate and logic circuit based on multistimuli-responsive raspberry-like micromotors. ACS Appl. Mater. Interfaces *8*, 15654–15660.

46. d'Ischia, M., Napolitano, A., Ball, V., Chen, C.-T., and Buehler, M.J. (2014). Polydopamine and eumelanin: from structure-property relationships to a unified tailoring strategy. Acc. Chem. Res. *47*, 3541–3550.

47. Nighswander-Rempel, S.P., Riesz, J., Gilmore, J., and Meredith, P. (2005). A quantum yield map for synthetic eumelanin. J. Chem. Phys. *123*, 194901.

48. Moreira, A.F., Gaspar, V.M., Costa, E.C., de Melo-Diogo, D., Machado, P., Paquete, C.M., and Correia, I.J. (2014). Preparation of end-capped pH-sensitive mesoporous silica nanocarriers for on-demand drug delivery. Eur. J. Pharm. Biopharm. *88*, 1012–1025.

49. Jin, X., Liu, C., and Zhang, H. (2019). Coccolith morphological and assemblage responses to dissolution in the recent sediments of the East China Sea. Mar. Micropaleontol. *152*, 101709.

50. Hassenkam, T., Johnsson, A., Bechgaard, K., and Stipp, S.L.S. (2011). Tracking single coccolith dissolution with picogram resolution and implications for CO2 sequestration and ocean acidification. Proc. Natl. Acad. Sci. USA *108*, 8571–8576.

51. Bucher, T., Clodt, J.I., Grabowski, A., Hein, M., and Filiz, V. (2017). Colour-value based method for polydopamine coating-stability characterization on polyethersulfone membranes. Membranes (Basel) *7*, E70.

52. Alkhaldi, M.H., Nasr-El-Din, H.A., and Sarma, H.K. (2010). Kinetics of the reaction of citric acid with calcite. SPE J. *15*, 704–713.

53. Soysal, O., Bahçeci, E., and Şahin, E. (2007). Aggregation in swarm robotic systems: Evolution and probabilistic control. Turk. J. Electr. Eng. Comput. Sci. *15*, 199–225.

54. Emilsson, G., Xiong, K., Sakiyama, Y., Malekian, B., Ahlberg Gagnér, V., Schoch, R.L., Lim, R.Y.H., and Dahlin, A.B. (2018). Polymer brushes in solid-state nanopores form an impenetrable entropic barrier for proteins. Nanoscale *10*, 4663–4669.

55. Tischer, T., Rodriguez-Emmenegger, C., Trouillet, V., Welle, A., Schueler, V., Mueller, J.O., Goldmann, A.S., Brynda, E., and Barner-Kowollik, C. (2014). Photo-patterning of non-fouling polymers and biomolecules on paper. Adv. Mater. *26*, 4087–4092.

56. Rodriguez-Emmenegger, C., Kylián, O., Houska, M., Brynda, E., Artemenko, A., Kousal, J., Alles, A.B., and Biederman, H. (2011). Substrate-independent approach for the generation of functional protein resistant surfaces. Biomacromolecules *12*, 1058–1066.

57. Barbey, R., Lavanant, L., Paripovic, D., Schüwer, N., Sugnaux, C., Tugulu, S., and Klok, H.-A. (2009). Polymer brushes via surface-initiated controlled radical polymerization: synthesis, characterization, properties, and applications. Chem. Rev. *109*, 5437–5527.

58. Paripovic, D., and Klok, H.-A. (2011). Improving the stability in aqueous media of polymer brushes grafted from silicon oxide substrates by surface-initiated atom transfer radical polymerization. Macromol. Chem. Phys. *212*, 950–958.

59. Tugulu, S., and Klok, H.-A. (2008). Stability and nonfouling properties of poly(poly(ethylene glycol) methacrylate) brushes under cell culture conditions. Biomacromolecules *9*, 906–912.

60. Kostina, N.Y., Pop-Georgievski, O., Bachmann, M., Neykova, N., Bruns, M., Michálek, J., Bastmeyer, M., and Rodriguez-Emmenegger, C. (2016). Non-fouling biodegradable poly(ε-caprolactone) nanofibers for tissue engineering. Macromol. Biosci. *16*, 83–94.

61. Alas, G.R., Agarwal, R., Collard, D.M., and García, A.J. (2017). Peptide-functionalized poly [oligo(ethylene glycol) methacrylate] brushes on dopamine-coated stainless steel for controlled cell adhesion. Acta Biomater. *59*, 108–116.

62. Rodriguez-Emmenegger, C., Preuss, C.M., Yameen, B., Pop-Georgievski, O., Bachmann, M., Mueller, J.O., Bruns, M., Goldmann, A.S., Bastmeyer, M., and Barner-Kowollik, C. (2013). Controlled cell adhesion on poly(dopamine) interfaces photopatterned with non-fouling brushes. Adv. Mater. *25*, 6123–6127.

63. Vorobii, M., de los Santos Pereira, A., Pop-Georgievski, O., Kostina, N.Y., Rodriguez-Emmenegger, C., and Percec, V. (2015). Synthesis of non-fouling poly[N-(2-hydroxypropyl)methacrylamide] brushes by photoinduced SET-LRP. Polym. Chem. *6*, 4210–4220.

64. Vorobii, M., Pop-Georgievski, O., de los Santos Pereira, A., Kostina, N.Y., Jezorek, R., Sedláková, Z., Percec, V., and Rodriguez-Emmenegger, C. (2016). Grafting of functional methacrylate polymer brushes by photoinduced SET-LRP. Polym. Chem. *7*, 6934–6945.

65. Ragni, R., Cicco, S.R., Vona, D., and Farinola, G.M. (2018). Multiple routes to smart nanostructured materials from diatom microalgae: A chemical perspective. Adv. Mater. *30*, e1704289.

66. Purcell, E.M. (1977). Life at low Reynolds number. Am. J. Phys. *45*, 3–11.

67. Mizukawa, Y., Miyashita, Y., Satoh, M., Shiraiwa, Y., and Iwasaka, M. (2015). Light intensity modulation by coccoliths of Emiliania huxleyi as a micro-photo-regulator. Sci. Rep. *5*, 13577.

68. Alfieri, M.L., Panzella, L., Oscurato, S.L., Salvatore, M., Avolio, R., Errico, M.E., Maddalena, P., Napolitano, A., and D'Ischia, M. (2018). The chemistry of polydopamine film formation: The amine-quinone interplay. Biomimetics (Basel) *3*, E26.

69. Paxton, W.F., Kistler, K.C., Olmeda, C.C., Sen, A., St Angelo, S.K., Cao, Y., Mallouk, T.E., Lammert, P.E., and Crespi, V.H. (2004). Catalytic nanomotors: autonomous movement of striped nanorods. J. Am. Chem. Soc. *126*, 13424–13431.

70. Li, W., Wu, X., Qin, H., Zhao, Z., and Liu, H. (2016). Light-driven and light-guided microswimmers. Adv. Funct. Mater. *26*, 3164–3171.

71. Chen, C., Mou, F., Xu, L., Wang, S., Guan, J., Feng, Z., Wang, Q., Kong, L., Li, W., Wang, J., and Zhang, Q. (2017). Light-steered isotropic semiconductor micromotors. Adv. Mater. *29*, 1–8.

72. Maggi, C., Saglimbeni, F., Dipalo, M., De Angelis, F., and Di Leonardo, R. (2015). Micromotors with asymmetric shape that efficiently convert light into work by thermocapillary effects. Nat. Commun. *6*, 7855.

73. Yang, M., and Ripoll, M. (2014). A self-propelled thermophoretic microgear. Soft Matter *10*, 1006–1011.